GRAVITATIONAL ORBIT-ATTITUDE COUPLING FOR VERY LARGE SPACECRAFT

G. B. SINCARSIN* and P. C. HUGHES**

Institute for Aerospace Studies, University of Toronto, 4925 Dufferin Street, Downsview, Ontario, Canada, M3H 5T6

(Received 25 August, 1982; accepted 25 May, 1983)

Abstract. Motion equations for the gravitationally coupled orbit-attitude motion of a spacecraft are presented. The gravitational force and torque are expanded in a Taylor series in the small ratio (spacecraft size/orbital radius). A recursive definition for higher moments of inertia is introduced which permits terms up to *fourth* order to be retained. The expressions are fully nonlinear in the attitude variables. A quasi-sun-pointing (QSP) passive attitude-control mode is used to assess the effects of higher moments of inertia and gravitational coupling. The attitude motion is detectably coupled to the orbital motion. However, the higher moments of inertia influence only the attitude motion.

Nomenclature

$\mathbf{f}_G, \mathbf{g}_G, \mathbf{f}_{Gi}, \mathbf{g}_{Gi}$	total gravitational force and torque and their components of order i in $\varepsilon = \rho/r_0$
$\mathbf{h}_0, \mathbf{h}_\oplus$	angular momentum of spacecraft about 0 and the spacecraft mass center
$\mathbf{J}^i, \mathbf{I}^i$	general moment of inertia about 0 and the spacecraft mass center
$\mathbf{J}, \boldsymbol{J}, \mathbb{J}, \mathbf{I}, \boldsymbol{I}, \mathbb{I}$	second (dyadic), third (triadic), and fourth (tetradic) moment of inertia about 0 and the spacecraft mass center
$\mathbf{J}^A, \mathbf{J}^B, \boldsymbol{J}^A, \boldsymbol{J}^B, \mathbb{J}^A, \mathbb{J}^B, \mathbb{J}^{AA}, \mathbb{J}^{AB}, \mathbb{J}^{BB}$	A and B (and related components) of the second, third and fourth moments of inertia about 0, see Equation (9)
M, m	Earth's mass, spacecraft mass
$\mathbf{Q}^{ba}$	rotation matrix taking $\mathcal{F}_a$ into $\mathcal{F}_b$
$\mathbf{r}, \mathbf{r}_0, \mathbf{r}_\oplus$	position vector from attracting body's mass center to a general mass element, to 0 and to the spacecraft mass center
$\boldsymbol{\alpha}_1, \boldsymbol{\alpha}_2, \boldsymbol{\alpha}_3$	basis vectors of reference frame $\mathcal{F}_\alpha$
$\beta, \Delta\beta, \beta_N$	misalignment angle between $\mathbf{b}_3$ and the (projected) true position of the Sun, its oscillatory component and nominal value
$\boldsymbol{\delta}$	unit dyadic ($\boldsymbol{\delta}$-identity matrix)
ε	ratio of characteristic spacecraft dimension to orbital radius
Θ	pitch angle (about $\mathbf{b}_2$ axis)
μ	Earth's gravitational parameter
$\boldsymbol{\rho}, \boldsymbol{\rho}_\oplus$	position vector from 0 to a general mass element and the spacecraft mass center
ψ, λ	the (projected) true longitude of the Sun and the true longitude of the spacecraft
$\boldsymbol{\omega}_{\alpha/\beta}$	angular velocity of reference frame $\mathcal{F}_\alpha$ with respect to $\mathcal{F}_\beta$
$(\cdot), (*), (^\circ)$	d( )/dt with respect to inertial space $\mathcal{F}_I$, and orbiting frame $\mathcal{F}_0$ and a body-fixed spacecraft frame $\mathcal{F}_b$

---

* Now Senior Research Engineer, Dynacon Enterprises Ltd., Member AIAA.
** Professor, Associate Fellow AIAA.
Presented at AAS/AIAA Astrodynamics Conference, Aug. 9–11, 1982.

Celestial Mechanics **31** (1983) 143–161. 0008–8714/83/0312–0143 $02.85.

1. Introduction

The motion of a satellite about an attracting body consists of two components: the orbital motion and the attitude. Typically, the orbit is assumed Keplerian and the spacecraft's attitude motion is studied independently. For purely gravitational interactions these motions are usually assumed to be uncoupled. While for most spacecraft this is a reasonable assumption, in reality the two motions are weakly coupled (gravitationally) such that a change in attitude will perturb the orbit and vice versa. The magnitude of this coupling is governed by the spacecraft's mass distribution and orientation, and its size relative to the orbital radius. Consequently, as future spacecraft increase in size the assumption of gravitational orbit-attitude de-coupling deserves closer examination.

The interdependence of the orbit and attitude motions is shown explicitly by expanding the differential gravitational force and torque in a Taylor series in the small parameter $\varepsilon = \rho/r_0$, where ρ is characteristic of the spacecraft size and r_0 is the orbital radius. Upon integrating over the spacecraft mass the resulting terms in both series contain moments of inertia of the spacecraft as well as the orbital radius. The usual practice is to neglect terms of order higher than ε^2. However, for much

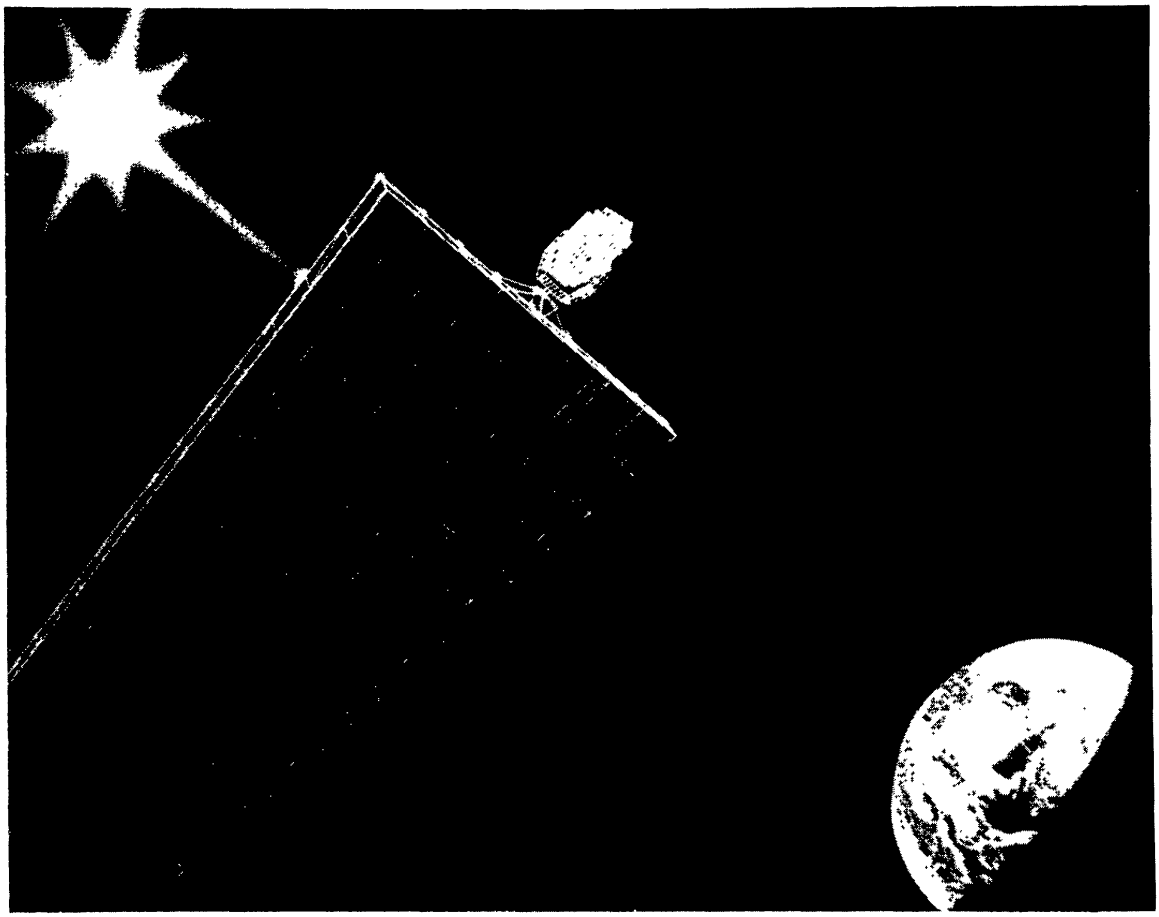

Fig. 1. Artist's conception of a solar power satellite.

larger spacecraft (see, for example, the proposed 10 km 'solar power satelite' in Figure 1), it is possible that higher-order terms should be included in studying the coupled problem. This possibility is explored in this paper.

2. Gravitational Force and Torque

2.1. Force and Torque on a Mass Element

The motion of a spacecraft about an attracting body possessing spherical mass symmetry is shown in Figure 2. The gravitational force acting on the element of mass $dm = \sigma(\boldsymbol{\rho})\, dv$ ($\sigma(\boldsymbol{\rho})$ is the mass density at $\mathbf{r}$ and dv is an element of volume) is

$$d\mathbf{f}_G = -\frac{\mu}{r^2}\hat{\mathbf{r}}\, dm, \tag{1}$$

where $\mu = GM$ is the gravitational parameter of the attracting body (G is the universal gravitational constant and M is the mass of the attracting body) and $\hat{\mathbf{r}} = \mathbf{r}/r$ is a unit

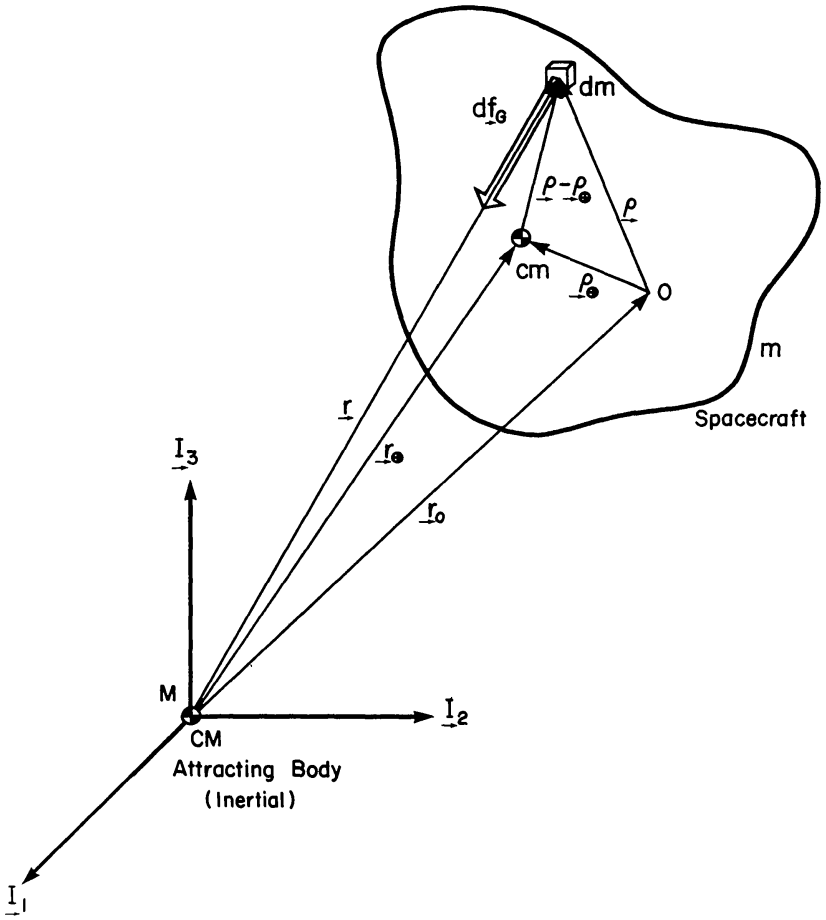

Fig. 2. Gravitational force on an elemental mass.

vector in the direction of $\mathbf{r}$. By observing that

$$\mathbf{r} = \mathbf{r}_0 + \boldsymbol{\rho} \tag{2}$$

($\boldsymbol{\rho} \ll r_0$), r^{-3} can be expanded in a Taylor series and along with (2) substituted into (1) to obtain

$$\begin{aligned} d\mathbf{f}_G \approx & -\frac{\mu}{r_0^2}\hat{\mathbf{r}}_0\, dm - \frac{\mu}{r_0^3}[\boldsymbol{\rho} - 3(\hat{\mathbf{r}}_0\cdot\boldsymbol{\rho})\hat{\mathbf{r}}_0]\, dm + \frac{\mu}{r_0^4}[3(\hat{\mathbf{r}}_0\cdot\boldsymbol{\rho})\boldsymbol{\rho} + \tfrac{3}{2}\rho^2\hat{\mathbf{r}}_0 - \\ & - \tfrac{15}{2}(\hat{\mathbf{r}}_0\cdot\boldsymbol{\rho})^2\hat{\mathbf{r}}_0]\, dm + \frac{\mu}{r_0^5}[\tfrac{3}{2}\rho^2\boldsymbol{\rho} - \tfrac{15}{2}(\hat{\mathbf{r}}_0\cdot\boldsymbol{\rho})^2\boldsymbol{\rho} - \tfrac{15}{2}(\hat{\mathbf{r}}_0\cdot\boldsymbol{\rho})\rho^2\hat{\mathbf{r}}_0 + \\ & + \tfrac{35}{2}(\hat{\mathbf{r}}_0\cdot\boldsymbol{\rho})^3\hat{\mathbf{r}}_0]\, dm - \frac{\mu}{r_0^6}[\tfrac{15}{2}(\hat{\mathbf{r}}_0\cdot\boldsymbol{\rho})\rho^2\boldsymbol{\rho} - \tfrac{35}{2}(\hat{\mathbf{r}}_0\cdot\boldsymbol{\rho})^3\boldsymbol{\rho} + \tfrac{15}{8}\rho^4\hat{\mathbf{r}}_0 - \\ & - \tfrac{105}{4}(\hat{\mathbf{r}}_0\cdot\boldsymbol{\rho})^2\rho^2\hat{\mathbf{r}}_0 + \tfrac{315}{8}(\hat{\mathbf{r}}_0\cdot\boldsymbol{\rho})^4\hat{\mathbf{r}}_0]\, dm. \end{aligned} \tag{3}$$

Here, terms up to $0(\varepsilon^4)$ are retained. For current spacecraft $\varepsilon \sim 10^{-7}$ (assuming a geostationary orbit). For very large spacecraft ($\rho \sim 10$ km) $\varepsilon \sim 10^{-4}$ is more typical. Indeed, this anticipated three-order-of-magnitude increase in ε in the next few decades motivates the retention of the higher-order terms in (3). For conventional spacecraft, only terms up to ε^2 are commonly retained [1, 2].

The gravitational torque acting on dm is given by

$$d\mathbf{g}_G = \boldsymbol{\rho} \times d\mathbf{f}_G. \tag{4}$$

To maintain mathematical consistency only terms of order ε^4 are retained in the expansion for $d\mathbf{g}_G$ after substitution of (3) into (4).

2.2. A RECURSIVE MOMENT-OF-INERTIA DEFINITION

Before integrating to obtain the total gravitational force and torque, it is necessary to introduce a compact vectorial moment-of-inertia definition compatible with the ε^3 and ε^4 terms implicit in (3) and the expansion of (4). This simplifies the formulation of the nonlinear equations governing the coupled orbit-attitude motion. A set of equations to fourth order in ε, but linear in the attitude variables, has been derived by Mohan [3] using a Lagrangian approach. Unlike the Newton-Euler approach adopted here, Mohan used scalar energy functions to formulate the motion equations. As a consequence the vector nature of the moment-of-inertia quantities intrinsic to the system can be obscured by numerous combinations of scalar components. It is not surprising, therefore, that the scalar moment-of-inertia quantities chosen by Mohan do not permit a convenient vectorial representation.

Meirovitch [4] however, suggests a scalar definition for higher-order moments of inertia which is readily represented in vectorial form;

$$\mathbf{J}^i = \int \boldsymbol{\rho}\boldsymbol{\rho}\ldots\boldsymbol{\rho}\, dm \qquad (i \text{ factors}), \tag{5}$$

where $\mathbf{J}^i$ is the ith moment of inertia about 0, $i > 2$. The scalar components of (5) are recovered by expressing the integrand as $\rho_\alpha \rho_\beta \dots \rho_\gamma$ (using cartesian tensor notation) and evaluating the integral for all possible combinations of $\alpha, \beta, \dots, \gamma \in (1, 2, 3)$. Only $\frac{1}{2}(i+1)(i+2)$ distinct scalar components exist for each $\mathbf{J}^i$. This also represents the number of integrations necessary to completely specify the ith moment of inertia. Unfortunately (5) is only partially compatible with the gravitational force and torque expansions and does not yield the familiar inertia dyadic for $i = 2$. The alternate, more compatible form developed here avoids this problem: Let

$$\mathbf{J}^1 = \int \boldsymbol{\rho}\, \mathrm{d}m = m\boldsymbol{\rho}_\oplus, \tag{6}$$

$$\mathbf{J}^2 = \int [(\boldsymbol{\rho}\cdot\boldsymbol{\rho})\boldsymbol{\delta} - \boldsymbol{\rho}\boldsymbol{\rho}]\, \mathrm{d}m. \tag{7}$$

Then define

$$\mathbf{J}^i = \int [\langle \mathbf{J}^{i-2} \rangle (\boldsymbol{\rho}\cdot\boldsymbol{\rho})\boldsymbol{\delta} - \boldsymbol{\rho}\boldsymbol{\rho}\langle J^{i-2} \rangle]\, \mathrm{d}m \qquad (i > 2), \tag{8}$$

where $\langle \mathbf{J}^i \rangle$ is the integrand of $\mathbf{J}^i$ and $\boldsymbol{\delta}$ is the unit dyadic ($\mathbf{J}^0 = \int \mathrm{d}m = m$). As the scalar components of (8) are simply linear combinations of the distinct components of (5) no extra integrations are involved. This recursive moment-of-inertia definition has been shown to be compatible with expansions for $\mathrm{d}\mathbf{f}_G$ and $\mathrm{d}\mathbf{g}_G$ up to at least sixth order in ε. Also, an extension of the parallel-axis theorem to third and fourth ($i = 3, 4$) moments of inertia is possible [5].

2.3. Force and Torque on a Body

The gravitational force and torque expressions shown in Table I are obtained by defining ($\mathbf{J}^2 \triangleq \mathbf{J}$, $\mathbf{J}^3 \triangleq \boldsymbol{J}$, $\mathbf{J}^4 \triangleq \mathbf{J}$)

$$\left.\begin{aligned}
&\mathbf{J}^A = \int \rho^2 \boldsymbol{\delta}\, \mathrm{d}m; \qquad \mathbf{J}^B = \int \boldsymbol{\rho}\boldsymbol{\rho}\, \mathrm{d}m \\
&\boldsymbol{J}^A = \int \rho^2 \boldsymbol{\rho}\boldsymbol{\delta}\, \mathrm{d}m; \qquad \boldsymbol{J}^B = \int \boldsymbol{\rho}\boldsymbol{\rho}\boldsymbol{\rho}\, \mathrm{d}m \\
&\mathbf{J}^{AA} = \int \rho^4 \boldsymbol{\delta}\boldsymbol{\delta}\, \mathrm{d}m; \qquad \mathbf{J}^{BB} = \int \boldsymbol{\rho}\boldsymbol{\rho}\boldsymbol{\rho}\boldsymbol{\rho}\, \mathrm{d}m \\
&\mathbf{J}^{AB} = \int \rho^2 \boldsymbol{\rho}\boldsymbol{\rho}\boldsymbol{\delta}\, \mathrm{d}m \\
&\mathbf{J}^A = \mathbf{J}^{AA} - \mathbf{J}^{AB}; \qquad \mathbf{J}^B = \mathbf{J}^{AB} - \mathbf{J}^{BB},
\end{aligned}\right\} \tag{9}$$

so that

$$\mathbf{J}^i = \mathbf{J}^{iA} - \mathbf{J}^{iB} \qquad (i = 2, 3, 4) \tag{10}$$

TABLE I
Gravitational force and torque expressions (to fourth order)

Force $\left(\mathbf{f}_G = \sum_{i=0}^{4} \mathbf{f}_{Gi}\right)$	Torque $\left(\mathbf{g}_G = \sum_{i=0}^{4} \mathbf{g}_{Gi}\right)$
$\mathbf{f}_{G0} = -\frac{\mu m}{r_0^2}\hat{\mathbf{r}}_0$	$\mathbf{g}_{G0} = \mathbf{0}$
$\mathbf{f}_{G1} = -\frac{\mu m}{r_0^3}[\boldsymbol{\rho}_\oplus - 3\hat{\mathbf{r}}_0\hat{\mathbf{r}}_0\cdot\boldsymbol{\rho}_\oplus]$	$\mathbf{g}_{G1} = \frac{\mu m}{r_0^2}\hat{\mathbf{r}}_0 \times \boldsymbol{\rho}_\oplus$
$\mathbf{f}_{G2} = \frac{\mu}{r_0^4}[3\mathbf{J}^B - \frac{3}{2}\hat{\mathbf{r}}_0\hat{\mathbf{r}}_0\cdot(\mathbf{J} - 4\mathbf{J}^B)]\cdot\hat{\mathbf{r}}_0$	$\mathbf{g}_{G2} = -3\frac{\mu}{r_0^3}\hat{\mathbf{r}}_0 \times \mathbf{J}^B\cdot\hat{\mathbf{r}}_0$
$\mathbf{f}_{G3} = \frac{\mu}{r_0^5}[\{\frac{3}{2}(\boldsymbol{J} - 4\boldsymbol{J}^B) - \frac{5}{2}\hat{\mathbf{r}}_0\hat{\mathbf{r}}_0\cdot(3\boldsymbol{J} - 4\boldsymbol{J}^B)\}\cdot\hat{\mathbf{r}}_0]\cdot\hat{\mathbf{r}}_0$	$\mathbf{g}_{G3} = -\frac{3}{2}\frac{\mu}{r_0^4}\hat{\mathbf{r}}_0 \times [(\boldsymbol{J} - 4\boldsymbol{J}^B)\cdot\hat{\mathbf{r}}_0]\cdot\hat{\mathbf{r}}_0$
$\mathbf{f}_{G4} = -\frac{\mu}{r_0^6}[(\{\frac{5}{2}(3\mathbf{J}^B - 4\mathbf{J}^{BB}) + + \frac{15}{8}\hat{\mathbf{r}}_0\hat{\mathbf{r}}_0\cdot[\mathbf{J} - 4(3\mathbf{J}^B - 2\mathbf{J}^{BB})]\}\cdot\hat{\mathbf{r}}_0)\cdot\hat{\mathbf{r}}]\cdot\hat{\mathbf{r}}_0$	$\mathbf{g}_{G4} = \frac{5}{2}\frac{\mu}{r_0^5}\hat{\mathbf{r}}_0 \times [\{(3\mathbf{J}^B - 4\mathbf{J}^{BB})\cdot\hat{\mathbf{r}}_0\}\cdot\hat{\mathbf{r}}_0]\cdot\hat{\mathbf{r}}_0$

and then integrating (3) and (4) over the spacecraft. $\mathbf{f}_{Gi}$ and $\mathbf{g}_{Gi}$ denote components of $\mathbf{f}_G$ and $\mathbf{g}_G$ containing terms of order i in ε. Alternately, the torque expansion given in the table can be obtained directly from the force expansion by observing that, given (2) and (4),

$$\mathbf{r}_0 \times \mathbf{f}_G = \int \mathbf{r} \times \mathrm{d}\mathbf{f}_G - \mathbf{g}_G. \tag{11}$$

However, since $\mathbf{r}$ and $\mathrm{d}\mathbf{f}_G$ are parallel, the integral vanishes. Consequently, after performing the cross-product operation in (11), only the non-$\hat{\mathbf{r}}_0\hat{\mathbf{r}}_0$ terms of $\mathbf{f}_G$ remain in $\mathbf{g}_G$.

$\mathbf{f}_{G1}$ might be said to represent the *gravity-gradient* force. Similarly, the gravity-gradient torque is $\mathbf{g}_{G2}$. Often, the point 0 (shown in Figure 2) is chosen to be the mass center. If so, both $\mathbf{f}_{G1}$ and $\mathbf{g}_{G1}$ vanish and the lowest-order perturbing force and torque are $\mathbf{f}_{G2}$ and $\mathbf{g}_{G2}$. These are the terms retained by previous analysts in their studies of the coupled orbit-attitude motion of spacecraft of the past two decades. Here, the intent to study very large spacecraft precipitates the inclusion of $\mathbf{f}_{G3}$, $\mathbf{f}_{G4}$, $\mathbf{g}_{G3}$, and $\mathbf{g}_{G4}$.

3. Role in Equations of Motion

The vectorial equations of motion for a very large spacecraft ($\mathbf{f}_G$ and $\mathbf{g}_G$ contain ε^4 terms) of constant mass m experiencing coupled orbit-attitude motion can be written in the form

$$m\ddot{\mathbf{r}}_{\oplus} = \mathbf{f}_G, \tag{12}$$

$$\dot{\mathbf{h}}_{\oplus} = \mathbf{g}_G - \boldsymbol{\rho}_{\oplus} \times \mathbf{f}_G. \tag{13}$$

Here, the attracting body is assumed to have a spherically symmetric mass distribution and $M \gg m$. Only gravitational perturbing forces and torques are included at present. However, additional disturbing functions (e.g., oblateness) can be incorporated readily. Now, letting $\boldsymbol{\omega}_{0/I}$ be the angular velocity of $\mathscr{F}_0$ (an orbital frame aligned with the instantaneous orbital radius and angular momentum vectors) relative to $\mathscr{F}_I$ (an inertial frame with origin at the attracting body's mass center), the orbit equation (12) becomes

$$\overset{**}{\mathbf{r}}_{\oplus} + \overset{*}{\boldsymbol{\omega}}_{O/I} \times \mathbf{r}_{\oplus} + 2\boldsymbol{\omega}_{O/I} \times \overset{*}{\mathbf{r}}_{\oplus} + \boldsymbol{\omega}_{O/I} \times (\boldsymbol{\omega}_{O/I} \times \mathbf{r}_{\oplus}) = \frac{1}{m}\mathbf{f}_G, \tag{14}$$

where $(^*)$ denotes differentiation with respect to $\mathscr{F}_0$. Given that the angular momentum about 0 is

$$\mathbf{h}_0 = \int \boldsymbol{\rho} \times \dot{\boldsymbol{\rho}}\, \mathrm{d}m = \mathbf{J} \cdot \boldsymbol{\omega}_{b/I} \tag{15}$$

while about the spacecraft's mass center $\oplus$ it is

$$\mathbf{h}_{\oplus} = \int \boldsymbol{\rho}_{\oplus} \times \dot{\boldsymbol{\rho}}_{\oplus}\, \mathrm{d}m = \mathbf{h}_0 - m\boldsymbol{\rho}_{\oplus} \times (\boldsymbol{\omega}_{b/I} \times \boldsymbol{\rho}_{\oplus}) \tag{16}$$

the attitude motion equation (13) can be transformed into

$$\mathbf{I} \cdot \mathring{\boldsymbol{\omega}}_{b/I} + \boldsymbol{\omega}_{b/I} \times (\mathbf{I} \cdot \boldsymbol{\omega}_{b/I}) = \mathbf{g}_G - \boldsymbol{\rho}_{\oplus} \times \mathbf{f}_G, \tag{17}$$

where the moment of inertia about $\oplus$ is

$$\mathbf{I} = \mathbf{J} - m(\rho_{\oplus}^2 \boldsymbol{\delta} - \boldsymbol{\rho}_{\oplus}\boldsymbol{\rho}_{\oplus}) \tag{18}$$

and $\boldsymbol{\omega}_{b/I}$ is the angular velocity of $\mathscr{F}_b$ (a body-fixed spacecraft frame) relative to $\mathscr{F}_I$. Differentiation with respect to $\mathscr{F}_b$ is represented by $(^\circ)$.

Details of the above procedure and the original motion equations are well known (see, for example, Hughes [6] or Meirovitch [7]). The unique aspect of (14) and (17) lies in the $\mathbf{f}_G$ and $\mathbf{g}_G$ terms. In particular, the compact vectorial moment-of-inertia definition adopted in the previous section enables the scalar equivalents of $\mathbf{f}_G$ and $\mathbf{g}_G$ (involving higher moments of inertia) to be expressed in a form fully nonlinear in the attitude variables. To the authors' knowledge, this capability is not presently available in the literature. The scalar expressions for a general spacecraft are not presented here (the interested reader is urged to consult [5]). Instead, for brevity, the special case of a planar spacecraft example (Figure 3) will be considered. Several proposed designs for futuristic antennas and solar power satellites have essentially this shape [8].

Two reference frames are shown in the figure, $\mathscr{F}_b$ and $\mathscr{F}_a$. The first is chosen to be the principal-axis frame whose origin coincides with the spacecraft mass center

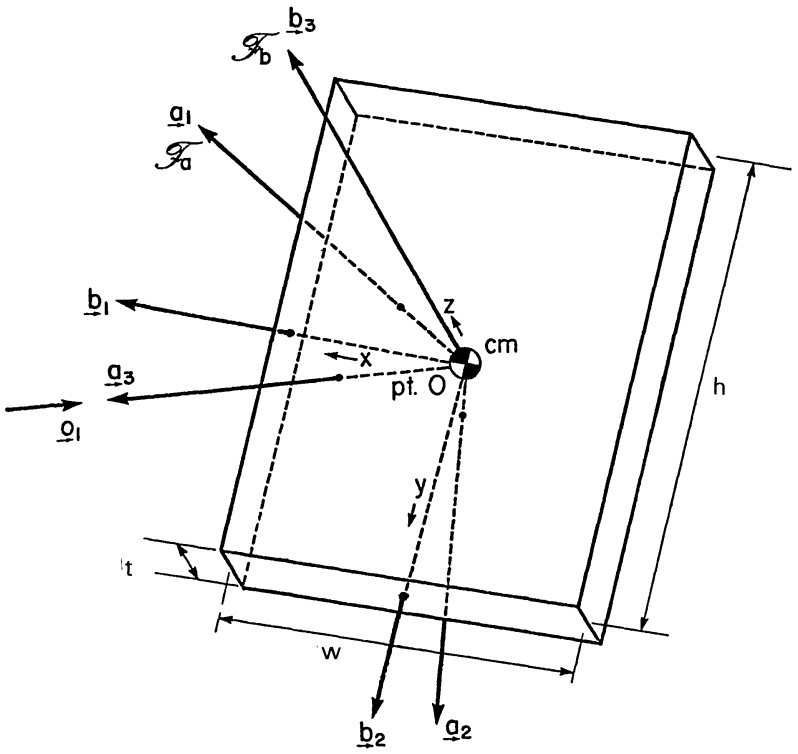

Fig. 3. Planar-form configuration.

(taken to be the point 0, i.e., $\rho_{\oplus} = 0$ and therefore $\mathbf{f}_{G1} = \mathbf{g}_{G1} \equiv \mathbf{0}$ and $\boldsymbol{J}^i \to \boldsymbol{I}^i$, $\boldsymbol{J} \to \boldsymbol{I}$, etc). The second, the attitude-reference frame, is related to $\mathscr{F}_0$ by a constant rotation. The orientation of $\mathscr{F}_b$ with respect to $\mathscr{F}_a$ determines the spacecraft's attitude (roll, pitch and yaw occur about $\mathbf{b}_1$, $\mathbf{b}_2$, and $\mathbf{b}_3$, respectively). Elements of the rotation matrix $\mathbf{Q}^{ba}$ taking $\mathscr{F}_a$ into $\mathscr{F}_b$ are denoted by Q^{ba}_{pq} $[p, q \in (1, 2, 3)]$.

The choice of $\mathscr{F}_b$ as a principal axis frame, of course, implies that $I_{ij} = 0$ for $i \neq j$, where I_{ij} $[i, j \in (1, 2, 3)]$ are the scalar components of $\mathbf{I}$ in $\mathscr{F}_b$. Several other inertia quantities vanish if the triaxially symmetric spacecraft shown in Figure 3 is assumed to have a uniform mass distribution $[\sigma(\boldsymbol{\rho}) \equiv \sigma$, a constant$]$. In particular, let (x, y, z) denote the components of $\boldsymbol{\rho}$ expressed in $\mathscr{F}_b$, where $|x| \leqslant w/2$, $|y| \leqslant h/2$, and $|z| \leqslant t/2$. Then odd functions of (x, y, z) after integration over $dm = \sigma dx\, dy\, dz$ become even and vanish over the cited symmetric intervals. Consequently, $\boldsymbol{I} = \boldsymbol{I}^A = \boldsymbol{I}^B \equiv \mathbf{0}$ and hence, $\mathbf{f}_{G3} = \mathbf{g}_{G3} \equiv \mathbf{0}$. Furthermore, several scalar components of $\mathbf{I}$ $[\mathbf{I}_{ijkm}, (i, j, k, m) \in (1, 2, 3)]$ also vanish. This leaves simply

$$\mathbf{f}_G = -\frac{\mu m}{r_0^2} + \mathbf{f}_{G2} + \mathbf{f}_{G4}; \qquad \mathbf{g}_G = \mathbf{g}_{G2} + \mathbf{g}_{G4}, \tag{19}$$

where the remaining scalar components for each term in (19) ($\mathbf{f}_G$ expressed in $\mathscr{F}_0$ and $\mathbf{g}_G$ in $\mathscr{F}_b$) are shown in Table II.

TABLE II
Gravitational force and torque for planar configuration

Force:

$$\begin{bmatrix} f_{G21} \\ f_{G22} \\ f_{G23} \end{bmatrix} = 3\frac{\mu}{r_\oplus^4}\begin{Bmatrix} \{I_{33} - \frac{1}{2}(I_{11}+I_{22})\} + \frac{3}{2}\{(I_{11}-I_{33})Q_{13}^{ba^2} + (I_{22}-I_{33})Q_{23}^{ba^2}\} \\ \{(I_{33}-I_{11})Q_{31}^{ba}Q_{37}^{ba}\} + \{(I_{22}-I_{11})Q_{21}^{ba}Q_{23}^{ba}\} \\ \{(I_{22}-I_{33})Q_{32}^{ba}Q_{33}^{ba}\} + \{(I_{22}-I_{11})Q_{12}^{ba}Q_{13}^{ba}\} \end{Bmatrix}$$

$$\begin{bmatrix} f_{G41} \\ f_{G42} \\ f_{G43} \end{bmatrix} = \frac{5}{2}\frac{\mu}{r_\oplus^6}\begin{Bmatrix} \frac{1}{4}[\{\Gamma_3 - 4(\Gamma_1+\Gamma_2)\} + 35\{[(\Gamma_1-\Gamma_3)+\Gamma_2(1-Q_{13}^{ba^2})]Q_{13}^{ba^2} + \\ \quad + [(\Gamma_2-\Gamma_3)+\Gamma_1(1-Q_{23}^{ba^2})]Q_{23}^{ba^2} - (\Gamma_1+\Gamma_2+\Gamma_3)Q_{13}^{ba^2}Q_{23}^{ba^2}\}] \\ \quad [\{4\Xi_{c1} - 7\Xi_{b1} - 11\Xi_{d2}\}Q_{31}^{ba}Q_{33}^{ba} - \\ \quad -7\{(\Xi_{b1}Q_{13}^{ba}Q_{11}^{ba} + 3\Xi_{d2}Q_{23}^{ba}Q_{21}^{ba} - \Xi_{a1}Q_{31}^{ba}Q_{33}^{ba})Q_{13}^{ba^2} + \Gamma_4 Q_{23}^{ba}Q_{21}^{ba} + \\ \quad + (3\Xi_{d1}Q_{13}^{ba}Q_{11}^{ba} + \Xi_{b2}Q_{23}^{ba}Q_{21}^{ba} - \Xi_{a2}Q_{31}^{ba}Q_{33}^{ba})Q_{23}^{ba^2}\}] \\ -[\{4\Xi_{c2} - 7\Xi_{b2} - 11\Xi_{d1}\}Q_{32}^{ba}Q_{33}^{ba} - \\ \quad -7\{(\Xi_{b2}Q_{23}^{ba}Q_{22}^{ba} + 3\Xi_{d1}Q_{13}^{ba}Q_{12}^{ba} - \Xi_{a2}Q_{32}^{ba}Q_{33}^{ba})Q_{23}^{ba^2} + \Gamma_4 Q_{13}^{ba}Q_{12}^{ba} + \\ \quad + (3\Xi_{d2}Q_{23}^{ba}Q_{22}^{ba} + \Xi_{b1}Q_{13}^{ba}Q_{12}^{ba} - \Xi_{a1}Q_{31}^{ba}Q_{33}^{ba})Q_{13}^{ba^2}\}] \end{Bmatrix}$$

Torque:

$$\begin{bmatrix} g_{G21} \\ g_{G22} \\ g_{G23} \end{bmatrix} = 3\frac{\mu}{r_\oplus^3}\begin{bmatrix} (I_{33}-I_{22})Q_{23}^{ba}Q_{33}^{ba} \\ (I_{11}-I_{33})Q_{13}^{ba}Q_{33}^{ba} \\ (I_{22}-I_{11})Q_{13}^{ba}Q_{23}^{ba} \end{bmatrix}$$

$$\begin{bmatrix} g_{G41} \\ g_{G42} \\ g_{G43} \end{bmatrix} = \frac{5}{2}\frac{\mu}{r_\oplus^5}\begin{bmatrix} [\{4\Xi_{c2} - 7\Xi_{b2} - 11\Xi_{d1}\} + 7\{(\Xi_{a1}+3\Xi_{d2})Q_{13}^{ba^2} + (\Xi_{a2}+\Xi_{b2})Q_{23}^{ba^2}\}]Q_{23}^{ba}Q_{33}^{ba} \\ -[\{4\Xi_{c1} - 7\Xi_{b1} - 11\Xi_{d2}\} + 7\{(\Xi_{a2}+3\Xi_{d1})Q_{23}^{ba^2} + (\Xi_{a1}+\Xi_{b1})Q_{13}^{ba^2}\}]Q_{13}^{ba}Q_{33}^{ba} \\ [\{7\Gamma_4 - 7[(3\Xi_{d2} - \Xi_{b1})Q_{13}^{ba^2} - (3\Xi_{d1} - \Xi_{b2})Q_{23}^{ba^2}]\}]Q_{13}^{ba}Q_{23}^{ba} \end{bmatrix}$$

where

$$\Xi_{ai} = I_{3333} - 2I_{i33i} - I_{33ii} \qquad \Gamma_1 = I_{1111} - 8I_{2332}$$
$$\Xi_{bi} = I_{iiii} - 2I_{i33i} - I_{ii33} \qquad \Gamma_2 = I_{2222} - 8I_{1331}$$
$$\Xi_{ci} = I_{3333} - I_{iiii} \qquad \Gamma_3 = I_{3333} - 8I_{1221}$$
$$\Xi_{di} = I_{1221} - I_{i33i} \qquad \Gamma_4 = \tfrac{11}{7}(I_{1111} - I_{2222}) + \tfrac{3}{7}(I_{2332} - I_{1331}) + (I_{2233} - I_{1133})$$

Each force and torque component in Table II is grouped in braces according to ascending order in the attitude variables. For example, consider the expansion for f_{G42}, which has two such groups. If the attitude motion were such that $\mathbf{Q}^{ba}$ differed only infinitesimally from the unit matrix (small attitude angles between $\mathcal{F}_b$ and $\mathcal{F}_a$), the first group in f_{G42} includes all the first-order attitude terms. The second brace group contains terms exclusively of second and higher order. As such, this term is neglected in a linear analysis. Here, the Euler parameters $(e_1, e_2, e_3, \bar{v})$, which satisfy the constraint $\mathbf{e}^T\mathbf{e} + v^2 = 1$, are chosen as attitude variables. Consequently, each Q_{pq}^{ba} consists of an algebraic combination of these parameters involving some nonlinearity. In other words, every Q_{pq}^{ba} in Table II generates some nonlinear attitude terms when written out explicitly. If a linear analysis is adopted, then these terms must also be neglected, however, the inertia quantities within a non-vanishing braced group remain unaltered.

4. Verification of Force and Torque Expansions

4.1. Analytical Verification

Two index patterns are noteworthy in Table II. (The same patterns and all that follows apply equally to a general spacecraft.) The first is skew-symmetry with respect to indices 1 and 2 in the second and third force components and the first and second torque components. The second is that the terms premultiplying $Q_{13}^{ba^2}$ and $Q_{23}^{ba^2}$ in the first force and third torque components obey the same index-switching rule (with the negative taken only for $\mathbf{g}_G$). These patterns lead to confidence in the cited expansions.

Another indication that Table II is correct is that the $\mathbf{g}_G$ components obtained from the expansion of (4) are reproduced by applying (11) directly to the $\mathbf{f}_G$ components from the table, on a term-by-term basis (i.e., for each order of ε). Unfortunately, this check does not explicitly involve the f_{Gk1} force components (where k is the order of ε in the terms retained) because the *radial* force component of $\mathbf{f}_G$ has no associated torque.

To rectify this situation the work of Mohan [3] was consulted. While his use of a Lagrangian approach makes it difficult to obtain $\mathbf{f}_G$ and $\mathbf{g}_G$ expansions fully nonlinear in the attitude variables, it is still possible to compare the linearized version of Table II with his equations. In fact, Mohan equations are reproduced [5] save for a minor discrepancy (believed notational) in the third-order moment-of-inertia terms (not shown here). To resolve this discrepancy an alternate source was sought. Meirovitch [4] provides a potential energy expression V (to order ε^4) which is helpful in this regard. Now, because $\mathscr{F}_0$ is herein defined so that its 1-axis lies along $\hat{\mathbf{r}}_0$ ($=\hat{\mathbf{r}}_\oplus$ for the chosen configuration) taking the gradient in terms of spherical coordinates implies that

$$f_{G1} = -(\partial V/\partial r_0), \tag{20}$$

where

$$f_{G1} = \sum_{k=0}^{4} f_{Gk1}; \quad f_{Gk1} = -(\partial V_k/\partial r_0) \tag{21}$$

and

$$V = \sum_{k=0}^{4} V_k. \tag{22}$$

After reconciling notational differences, the f_{Gk1} components from this procedure were shown to be identical to those given in Table II [5].

4.2. Numerical Verification

Based on the equations of the previous section, a FORTRAN computer simulation (~ 3700 lines) was written to study numerically the effects of including higher

moments of inertia. This also afforded an opportunity to numerically verify the expressions in Table II by comparison with analytical predictions. Again, the work of Mohan [3] proves useful. For the chosen configuration (recall Figure 3), the notational controversy cited above is of no consequence, as $\mathbf{f}_{G3} = \mathbf{g}_{G3} \equiv \mathbf{0}$. Recall, however, that while Mohan's equations are linear in the attitude variables, those used here are not.

The situation chosen for comparison involves an energy transfer between the in-plane orbital motion and pitch attitude motion of a spacecraft. As shown schematically in Figure 4, first the pitch oscillations Θ slowly subside while the mean orbital eccentricity e increases; indeed the pitch amplitude is zero when the mean eccentricity is at its maximum value. Then the reverse takes place: the eccentricity decreases while the pitch amplitude increases to its original value. This beating phenomenon, caused because the period of the pitch oscillations and the orbital period are approximately equal, repeats itself. Since the two motions are only weakly coupled, energy slowly transfers from one type of motion to the other. While the analytical predictions which follow are based on the mean motion, the present simulation actually produces the detailed motion shown in Figure 4.

Mohan predicts that e reaches its maximum value

$$e_{\max} = |\Theta_0 \sqrt{\xi}| \tag{23}$$

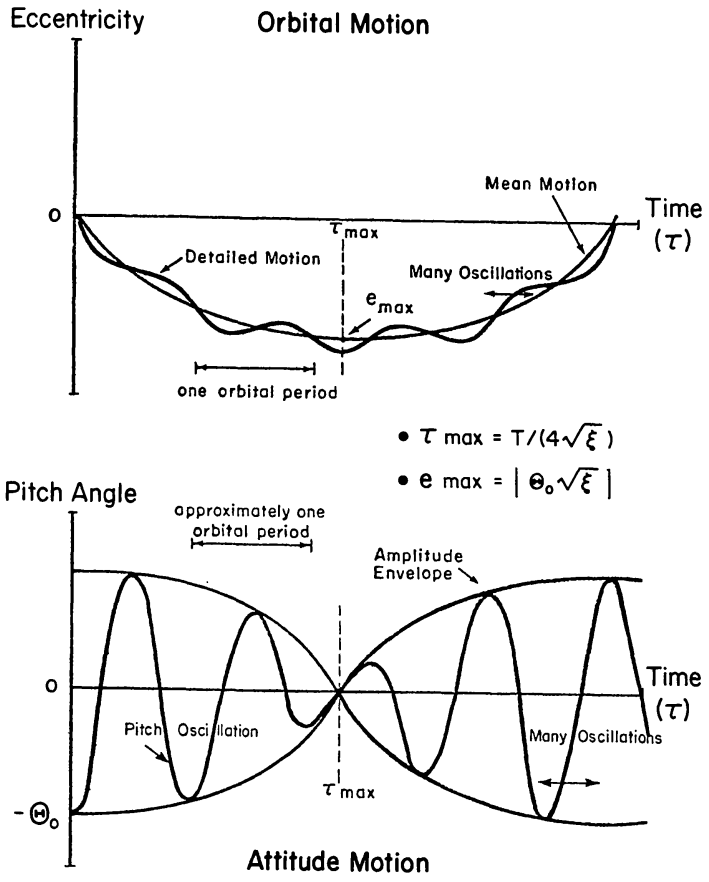

Fig. 4. Schematic of pitch-in-plane motion.

at time

$$\tau_{max} = T/(4\sqrt{\xi}), \tag{24}$$

where T is the orbital period and Θ_0 is the initial pitch angle. $\sqrt{\xi}$ is an inertia parameter, characteristic of the spacecraft:

$$\xi = \frac{\mu}{n^2 m R^5}\left[3(I_{11} - I_{33}) - \frac{5}{2}\frac{\{4\mathcal{I}_{3333} + 11(\mathcal{I}_{2332} - \mathcal{I}_{1111} - I_{1221}) + 7(2\mathcal{I}_{1331} + I_{1133})\}}{R^2}\right] \tag{25}$$

with

$$n^2 = \frac{\mu}{R^3}\left[1 - \frac{3}{2}\frac{(2I_{33} - I_{11} - I_{22})}{mR^2} - \frac{5}{8}\frac{\{\mathcal{I}_{3333} - 4(\mathcal{I}_{1111} + I_{2222}) + 32(\mathcal{I}_{1331} + \mathcal{I}_{2332}) - 8\mathcal{I}_{1221}\}}{mR^4}\right], \tag{26}$$

R is the orbital radius of the reference orbit (the orbit in absence of any disturbances) and n is the mean angular velocity of this orbit (taken to be circular). Implicit in (23) and (24) are the assumptions that Θ be small and that $\chi\,(= \Theta_0/\sqrt{\xi}) \gg 1$. A comparison of the predicted and simulated results for e_{max} and τ_{max} is shown in Table III, for $\Theta_0 = = 0.5$ deg and $\chi = 10, 11$. The agreement is always, better than 10% and improves proportionally with an increase in χ. The resulting motion is indeed as characterized in Figure 4; the eccentricity reaches its maximum as simultaneously the pitch oscillation amplitude becomes zero. Relatively small values of χ were chosen to minimize computational time ($\sim \tau_{max}$) while maximizing e_{max} through an appropriate choice for ξ.

TABLE III
Results of comparison with Mohan [3]

	τ_{max}, yr		
χ	Predicted	Simulated	Difference (%)
10	0.783	0.709	9.4
11	0.857	0.784	8.5

	$e_{max}(\times 10^{-6})$		
χ	Predicted	Simulated	Difference (%)
10	7.61	7.86	3.3
11	6.95	7.12	2.4

No numerical results for nonlinear attitude effects in conjunction with higher moments of inertia are available in the literature. The simple check of repeating the above comparison with the simulation in a *nonlinear* mode was, however, performed. The results commonly differ from their linear counterparts in the fifth and sixth significant digits. As roll and yaw are initially quiescent and no out-of-plane disturbances are present – a condition in which pitch and roll-yaw decouple – it is reassuring that no roll-yaw attitude or out-of-plane orbital perturbations were excited numerically. The simulation was also shown to reproduce, to more than ten significant digits, the exact analytical solution to the nonlinear pitch equation

$$I_{22}\ddot{\Theta} + 3\omega_c^2(I_{11} - I_{33}) \sin \Theta \cos \Theta = 0. \tag{27}$$

A circular orbit, with radius r and a constant angular velocity $\omega_c = (\mu/r^3)^{1/2}$, was assumed. Also, the coupling of pitch into the orbit and higher-order moments of inertia (which preclude an exact analytical solution) were neglected.

Numerical results for coupled out-of-plane (orbital) and roll-yaw (attitude) motions similar to those for the in-plane-pitch system are absent in the literature as these motions occur only near the stability boundaries for the coupled system [2], a region where no practical satellite would be designed. Consequently, no numerical comparisons could be made for this type of coupled motion.

5. Numerical Results

5.1. A QUASI-SUN-POINTING ATTITUDE MODE

Prior to discussing the numerical results it is timely to describe briefly the passive attitude mode in which the spacecraft is placed. A quasi-inertial stabilization scheme whereby a spacecraft in a circular orbit slowly tumbles about the orbit normal, while at least one principal axis remains in the orbit plane, was introduced by Elrod in 1972 [9]. The tumbling occurs in the direction opposite to the orbit motion so that, by correctly choosing the tumbling period, the spacecraft can be made to appear motionless, on average, to an inertial observer. In truth, gravitational perturbing torques cause small attitude oscillations relative to inertial space (up to 18.8°). Hence the name *quasi-inertial.*

It is straightforward to introduce a small secular term into this motion, by changing slightly the period of the tumbling motion [5]. Thus a spacecraft in ecliptic orbit can be made to track the sun (on average) over one tropical year, rather than remaining stationary relative to an inertial observer. For an equatorial orbit, the projection of the Sun's true position on the equatorial plane can be tracked (on average, over one year). As before, however, gravitational perturbing torques induce an attitude oscillation relative to the nominal (per oscillation) pointing direction β_N. The ampli-

tude of the oscillation $\Delta\beta$ is not significantly greater than that experienced in the quasi-inertial mode (the maximum amplitude is 18.9°). Mathematically,

$$\begin{aligned}\beta &= (\psi - \lambda) + \Theta \\ &= \beta_N + \Delta\beta\end{aligned} \tag{28}$$

and

$$\int_{t_0}^{t_0+1\text{ yr}} \beta_N \, dt = 0, \tag{29}$$

where ψ is (the projection of) the true longitude of the Sun for a spacecraft in (equatorial) ecliptic orbit and λ is the true longitude of the spacecraft, both measured relative to the vernal equinox ($t_0 = 0$). Recall that Θ is the pitch angle. Also, the spacecraft is assumed to maintain the pitch axis $\mathbf{b}_2$ perpendicular to the orbital plane. β is simply the angle between the (projected) true position of the Sun and the principal axis confined to the orbital plane, $\mathbf{b}_3$, for the present spacecraft (ideally $\beta \equiv 0$). This extension to Elrod's quasi-inertial mode will henceforth be designated as the *quasi-sun-pointing* (QSP) attitude mode.

5.2. Description of Study

The QSP mode offers an opportunity to study a plausible highly nonlinear attitude motion which can also be practical for certain sun-pointing missions. The solar power satellite highlighted here (another is also considered in [5]) is a limiting example for this mode and illustrates the worst case. The intent is to ascertain the effects of higher moments of inertia. Based on the dimensions [10] and inertia properties for the chosen spacecraft (see Table IV) it can be argued that, even for this very large spacecraft, the effect of $\mathbf{f}_{G4}$ will be minimal, assuming a geostationary orbit. Con-

TABLE IV
Physical properties of solar power satellite example

Dimensions (km)									
		h	13.1						
		w	4.93						
		t	0.21						
Moments of inertia									
Zeroth order, $\times 10^6$ kg		Second order, $\times 10^8$ kg km^2		Fourth order, $\times 10^7$ kg km^4					
m	18.06	I_{11}	2.58	I_{1111}	665	I_{2211}	−599	I_{3311}	783	I_{1221}	52.3
		I_{22}	0.367	I_{1122}	704	I_{2222}	13.4	I_{3322}	783	I_{1331}	0.0134
		I_{33}	2.95	I_{1133}	652	I_{2233}	−651	I_{3333}	783	I_{2332}	0.0949

sequently, it is neglected here. While this may appear somewhat inconsistent in that $\mathbf{g}_{G4}$ is retained [recall Equation (19)], the resulting system, in fact, contains the first perturbations caused by gravity in each type of motion. That is, $\mathbf{f}_{G2}$ is to $\mathbf{f}_{G0}$ as $\mathbf{g}_{G4}$ is to $\mathbf{g}_{G2}$.

The numerical procedure adopted involves progressively increasing the amount of coupling between the orbital and attitude dynamics. As illustrated in Figure 5, initially a Keplerian orbit is considered, with the orbit 'driving' the attitude through the gravity-gradient torque $\mathbf{g}_{G2}$. The loop is then closed by the addition of $\mathbf{f}_{G2}$, whereby the attitude now perturbs the orbit. This is commonly known as the 'coupled problem'. Finally, higher moments of inertia are included by 'balancing' the perturbations in the system with the addition of $\mathbf{g}_{G4}$ to the attitude dynamics.

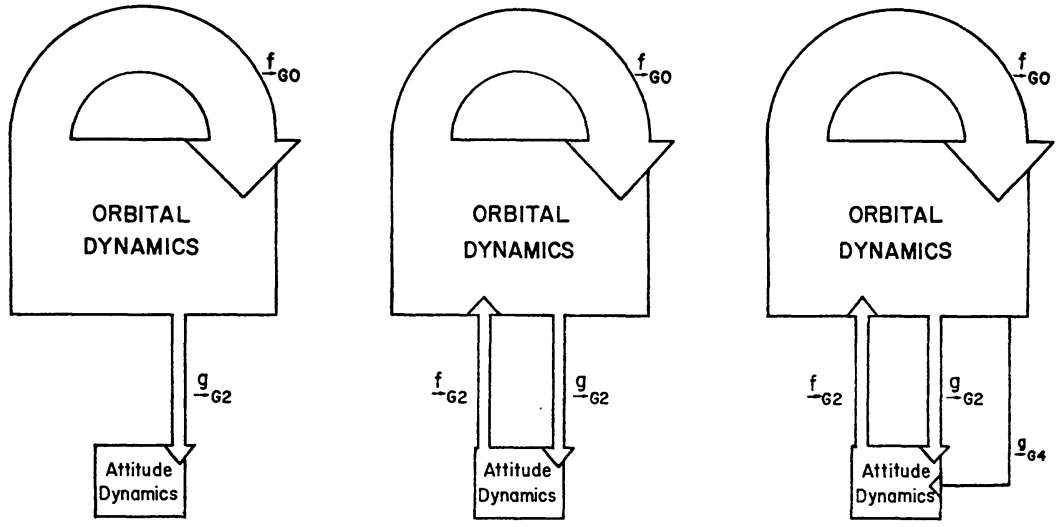

(a) Keplerian Orbit and Gravity - Gradient Torque ($\underline{g}_{G2}$) Only

(b) The Coupled Problem: Orbit Affected by Attitude Motion

(c) 'Balanced' Coupling (Depends on Higher Moments of Inertia)

Fig. 5. Progressively more accurate models of the gravitational coupling between orbital dynamics and attitude dynamics.

The typical run duration is one tropical year, while the period of the equatorial-QSP mode at geostationary altitude is one mean solar day. Consequently, 365.2422 QSP periods occur for each run. Rather than obscure the numerical results by plotting all of these periods only eight periods, spaced at 46-day intervals, are selected. Essentially they correspond to the equinoxes (day 1 is the vernal equinox), the solstices and the days midway between. The plot of each selected period has timing symbols located at 1.2 mean solar hour intervals. Also, the start (S) and finish (F) of each period is noted, with increasing time indicated by arrowheads.

5.3. Attitude Results

Since $\mathbf{g}_{G4}$ directly affects the attitude motion (while only indirectly influencing the orbit) one might expect the most prominent effects from the higher moments of in-

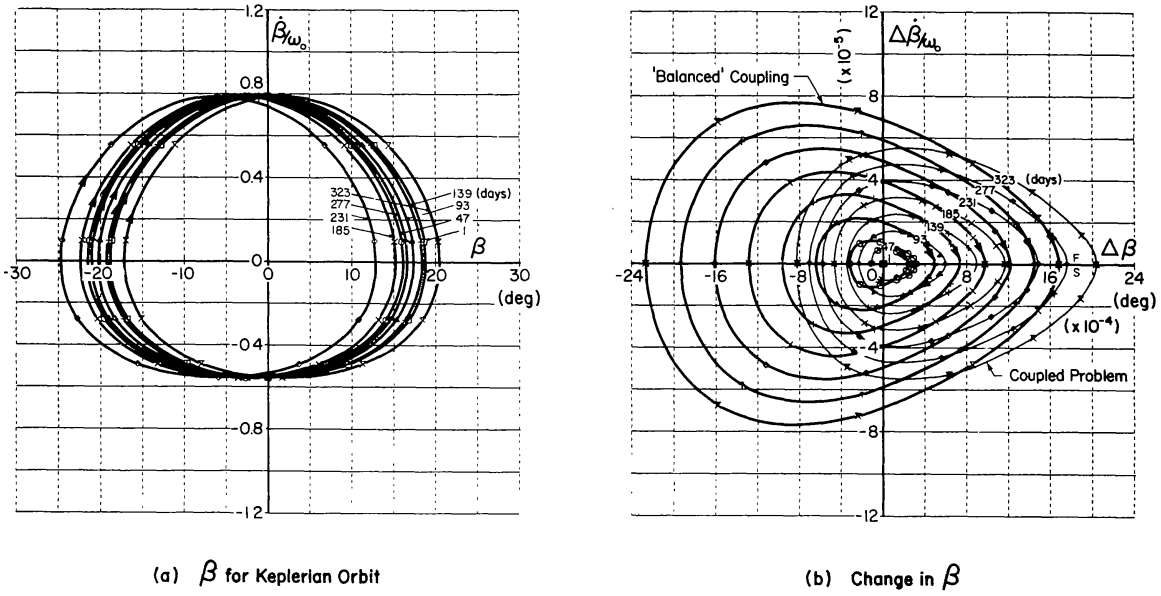

Fig. 6. Effects of gravitational coupling and higher moments of inertia on the QSP (quasi-sun-pointing) passive mode.

ertia to occur in the attitude variables. The actual effect of $\mathbf{g}_{G4}$ is shown in Figure 6b. The change in β caused by this torque is of the same order of magnitude as the β-variation caused by initially coupling the attitude into the orbit (Figure 6a shows β prior to coupling). A close examination reveals this variation is predominantly a small shift in phase of the oscillatory component of β, with some distortion in amplitude (Figure 6b). The addition of $\mathbf{g}_{G4}$ changes the degree of distortion and consequently modifies the magnitudes caused by the phase shift. Figure 6b also shows the effect of coupling to be cumulative with the change at a given $(\Delta\beta, \Delta\dot{\beta}/\omega_0)$ point constant from period to period, even though within a given day β and $\dot{\beta}/\omega_0$ vary at different rates ($\omega_0 = \omega_c - \omega_s$, where $\omega_c = \pi/2$ rad/sid-hr and ω_s is the mean angular velocity of the Sun).

5.4. Orbital Results

To completely ascertain the effect of higher moments of inertia in the coupled problem (for the chosen spacecraft), it remains to consider the changes experienced by the orbit. Coupling the attitude into the orbit causes changes in the inplane orbital elements: the semi-major axis a, the eccentricity e, the argument of periapsis ω, and the true anomaly v. The inclination i and the longitude of the ascending node Ω remain unchanged. (Prior to coupling $a = 42\,164$ km, $e = i = 0$, and Ω, ω, and v are undefined.) The variations in the semi-major axis and the eccentricity are shown in Figure 7. A polar format is used whereby the change in a and e (relative to their initial values) is plotted radially versus the true longitude λ ($= \Omega + \omega + v$, Ω set to zero) of the spacecraft. This displays the results relative to inertial space over the run duration of one year.

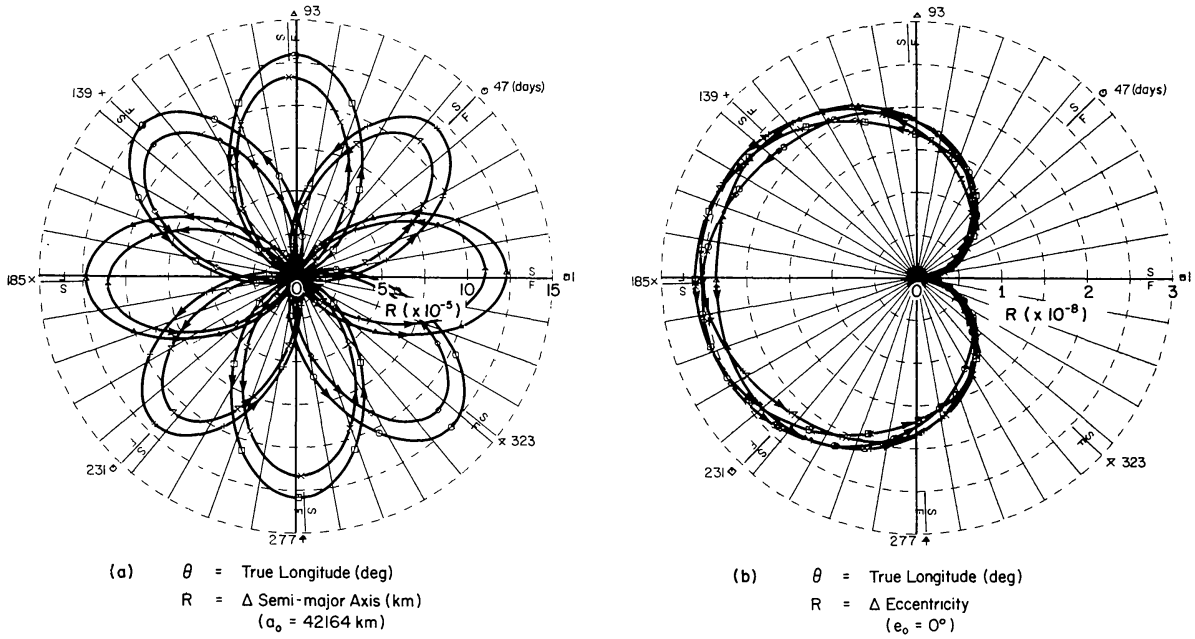

Fig. 7. Typical perturbations to the orbital motion from the attitude motion.

The variation in the direction of the periapsis relative to inertial space (not shown) is almost independent of the day on which a particular β-oscillation begins. Nominally, it sweeps through approximately 120° per orbit. However, atypical variations in ω occur near the beginning ($\lambda = 0°$) and the end ($\lambda = 360°$) of each orbit. These variations appear related to the phase difference between the orbit and attitude motions relative to inertial space. The days that form period pairs (1, 185), (47, 231), (93, 277) and (139, 323) have the same phase difference and show very similar ω-variations. The eccentricity displays the same tendencies (Figure 7b). These are relatively independent of the chosen day; however, some attitude dependence is present, with the period-pairs cited above in evidence. A strong dependence on orbital position is observed. Also, no long-term buildup in e occurs. The variations observed in the semi-major axis (Figure 7a) also suggest that no e-β-type beating is present for this coupled problem. The double-lobe pattern shown in the figure results from a transfer of energy between the attitude and orbit over each quarter-period of the β-oscillation; over the first quarter-period the orbit gains energy and the attitude loses energy; over the second quarter-period the reverse occurs; and the process repeats itself over the third and fourth quarter-periods. This corresponds directly to changes in the specific orbital energy $\mathscr{E} = -\mu/2a$. The amount of energy transferred between the attitude and orbit is a constant over one year.

The inclusion of $\mathbf{g}_{G4}$ in the attitude equations does not produce any appreciable changes to the variations in the orbital elements. Changes that were noted appeared random and were of the order of the numerical precision possible with the given simulation (16 significant digits).

5.5. Numerical accuracy

The reduction, between periods, of the lobes shown in Figure 7a implies that energy has been lost from a conservative system. This loss of energy is caused by numerical error; however, it represents only a $5 \times 10^{-8}\%$ change in the total energy over an entire year and 439 200 integration steps! This is equivalent to a reduction in the orbital period of 7×10^{-5} s. Such a high degree of accuracy is also supported by the extent to which the orbital (see Figure 8) and attitude Euler parameter constraints are satisfied (recall $\mathbf{e}^T\mathbf{e} + \bar{\nu}^2 = 1$). (For computational reasons [11], Euler parameters were also adopted as orbital variables, although the numerical results are displayed in classical orbital elements to aid visualization.) These constraints are maintained to within 10^{-14}, the machine accuracy possible for a differencing operation using IBM double precision arithmetic. It is reasonable to assume, therefore, that the remaining state variables (the orbital radius, the in-plane velocity components and the components of the angular momentum associated with the attitude motion) are also determined very accurately, given that they are obtained using the same integration scheme and that they are less rapidly varying. All of this suggests that the simulation is achieving its numerical limit.

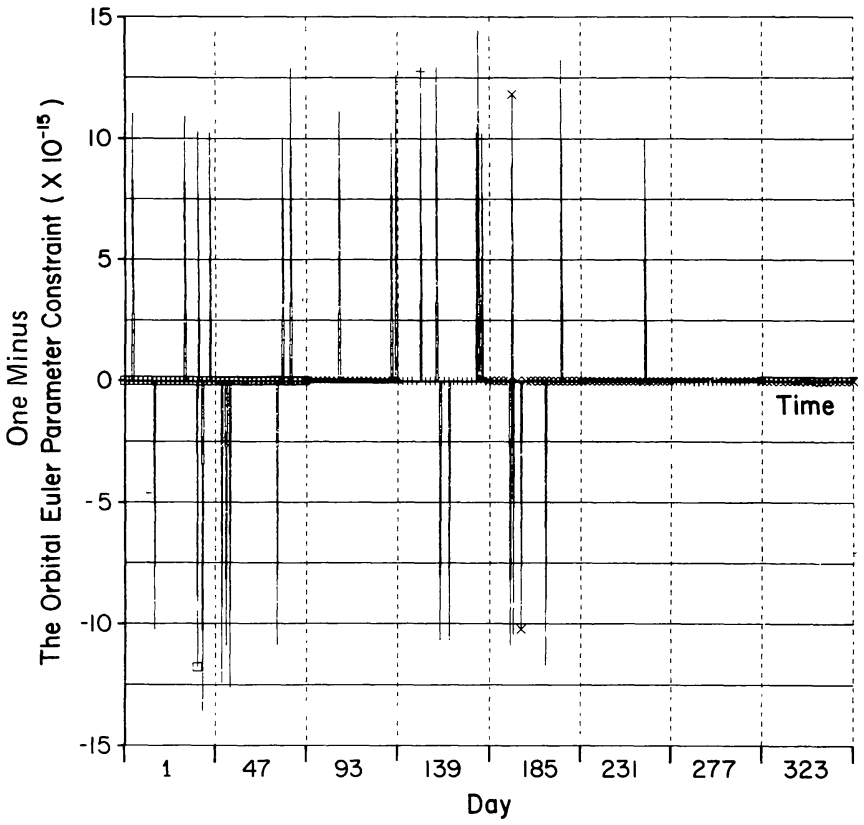

Fig. 8. Typical orbital Euler parameter errors.

6. Conclusions

Measurable variations in both the orbital and attitude variables occur when the (small) gravitational coupling between orbital and attitude dynamics is included in the simulation. However, only the attitude motion is changed significantly by the inclusion of higher moments of inertia. This change is predominantly a shift in phase of the oscillation characteristic of the QSP mode. Orbital variations are restricted to the in-plane elements: semi-major axis, eccentricity, argument of periapsis and true anomaly. The observed phase shift and orbital perturbations are too small to present a serious control problem. However, an accurate representation of these gravitationally induced coupled-orbit-attitude perturbations requires the retention of higher moments of inertia.

Care should be taken not to indiscriminately neglect the contributions from higher moments of inertia for all very large spacecraft applications; their importance should be assessed on an individual basis.

Acknowledgement

This work was sponsored by the Natural Sciences and Engineering Research Council of Canada under Grant No. A4183.

References

1. Mohan, S. N., Breakwell, J. V., and Lange, B. O.: 1972, 'Interaction Between Attitude Libration and Orbital Motion of a Rigid Body in a Near Keplerian Orbit of Low Eccentricity', *Celest. Mech.* **5**, 157–173.
2. Lange, B. O.: 1970, 'Linear Coupling Between Orbital and Attitude Motions of a Rigid Body', *J. Astronaut. Sci.* **XVIII**, No. 3, 150–167.
3. Mohan, S. N.: 1970, 'Orbital Perturbations Due to Attitude Libration of an Arbitrary Rigid Body Moving in a Central Newtonian Field', Dept. of Aeronautics and Astronautics, Stanford University, SUDAAR Rep. No. 410.
4. Meirovitch, L.: 1968, 'On the Effect of Higher-Order Inertia Integrals on the Attitude Stability of Earth-Pointing Satellites', *J. Astronaut. Sci.* **XV**, No. 1, 14–18.
5. Sincarsin, G. B.: 1982, 'Gravitational Orbit-Attitude Coupling and Penumbral Solar-Gradient Torques for very Large Spacecraft', UTIAS Report 265.
6. Hughes, P. C.: 1984, *Spacecraft Attitude Dynamics*, (to be published).
7. Meirovitch, L.: 1970, *Methods of Analytical Dynamics*, McGraw-Hill, New York.
8. Woodcock, G. R.: 1977, 'Solar Satellites–Space Key to Our Power Future', *AIAA Astronaut. Aeronaut.* **15**, No. 7/8, 30–43.
9. Elrod, B. D.: 1972, 'A Quasi-Inertial Attitude Mode for Orbiting Spacecraft', *J. Spacecraft Rockets* 9, No. 12, 889–895.
10. Glaser, P. E.: 1977 'The Potential of Satellite Solar Power', *Proc. IEEE* **65**, No. 8, 1162–1176.
11. Sincarsin, G. B.: 1982, 'Simulation of Solar Radiation Pressure Torque on a Satellite in Earth's Penumbra', *Proceedings 10th IMACS World Congress on System Simulation and Scientific Computation*, Montreal, Canada, Aug. 8–13.